Antenna-Coupled Graphene Josephson-Junction Terahertz Detector

F. Javier Gonzalez,[1] Michael S. Lodge,[2] Masahiro Ishigami,[2,3] Richard A. Klemm,[2] Ami Rathod,[2] Kirsten L. Lina,[2] Anna C. Bowman,[2] Francisco Hernandez,[2] Chris J. Fredricksen,[1] Coleman Cariker,[1] R. E. Peale[1,2,*]

[1]Truventic LLC, 1209 W. Gore St. Orlando FL 32816, [2]Physics Department, University of Central Florida, Orlando FL 32816, [3]Nanoscience Center, University of Central Florida, Orlando FL 32816, *robert.peale@ucf.edu

Abstract

Highly sensitive, broadly tunable detectors are needed for future sensing applications and quantum information systems. A promising material for these challenges comprises stacked graphene sheets having a "magic" twist angle between their in-plane symmetry axes. This material displays superconductivity with a ~ 2K transition temperature. We investigate the possibility of fast and sensitive detectors for THz and mm-waves by integrating magic angle graphene Josephson junctions with antennas. The considered detection mechanism is based on the decrease in the maximum zero-voltage DC current when AC current is driven through the junction. Bowtie, log-periodic, square spiral, and Archimedean spiral antennas were analyzed by finite element simulation. The bowtie gave the highest current at the feed at THz frequencies. Responsivity, noise-equivalent-power, and the prospects for single-photon detection are estimated.

Introduction

Highly sensitive and broadly tunable detectors are needed for low-light sensing and quantum information systems. The former application benefits from high sensitivity and wavelength selectivity. The latter application often demands both single-photon sensitivity and high speed [1]. Single photon detector development has been mainly at wavelengths shorter than the near-infrared. Emerging 5G and 6G (mm-wave to THz) technologies offer an interesting new spectral domain for quantum information systems. A single photon detector of mm-waves to low-THz has been suggested recently for this application [2].

Single photon detectors need to be both sensitive and fast [1]. An opportunity for a fast and sensitive THz to mm-wave detector is a video detector based on antenna-coupled, twisted-graphene superconducting Josephson junctions (JJ). JJs have both video and bolometric detection mechanisms, both of which can be very sensitive, but the former has "very great speed advantage over the bolometer" [3].

A "magic" twist angle between graphene sheets flattens the electronic band structure near the Dirac point, creating a high density of states and the possibility of superconductivity [4]. The superconducting transition temperature is ~2 K for 2 - 4 layers [4]. Superconducting graphene JJs have been demonstrated [4]. This paper considers the possibility of creating ultrasensitive detectors of THz and mm-waves by coupling such JJs to antennas.

Results

To illustrate the detection mechanism, Figure 1(left) presents JJ Voltage-Current (VI) curves replotted from [4]. In the video detector mechanism, the maximum zero voltage current, I_1, is depressed when an AC voltage appears across the JJ. Such a voltage appears when an AC current is driven through a JJ load, sourced by an antenna, because the AC impedance is non-zero even when the DC resistance is zero. The device is current biased at the dark value of I_1. When mm-waves or THz are absorbed by a suitable antenna with the JJ at its feed, I_1 shifts below the bias point, and a DC voltage appears across the JJ. The sensitivity of the device is due to the steepness of the VI curve at the bias point.

The I_1 value shifts similarly with increasing temperature, giving rise to the bolometric mechanism, which can be very sensitive. However, for such thermal detectors, speed and sensitivity are mutually exclusive. Sensitive-but-slow bolometers are of interest for low-light sensing, but we consider only the video detector mechanism in this short paper.

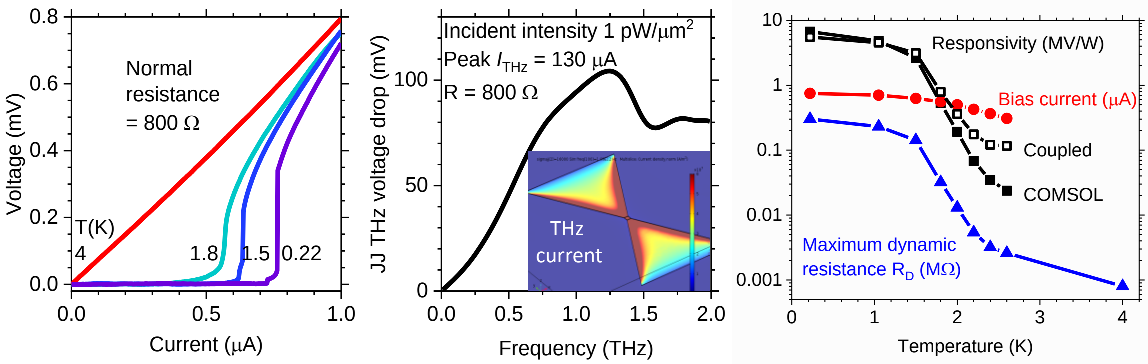

Fig. 1 (left) VI curves from [4] for JJ at indicated temperatures. (right) Spectrum of induced THz voltage drop across JJ load. Inset: THz current distribution in antenna.

The resistively shunted junction (RSJ) model for JJ detectors comprises an ideal junction with only pair tunnelling current and a parallel shunt resistor R that carries only quasiparticle current. The value of R is the normal state resistance [3], which according to Fig. 1 (left) is 800 Ω. THz photon energies exceed the superconducting gap, so THz currents pass mainly through R. Additional inductive reactance determined from the Josephson equations [3] depends on AC current, so its estimation is complicated. We assume R, the lower bound on impedance, for our responsivity estimates. Among bowtie, log-periodic, square spiral, and Archimedean spiral antennas, the bowtie gives the highest THz electric field at the feed, and hence should give the highest responsivity. Fig. 1 (center) presents COMSOL simulation results for 1 pW/μm^2 incident power.

The shift $\delta I_1 = -(2eV_{THz}/\hbar\omega)^2 I_1/4$, according to [1,5]. The squared factor is the ratio of the pair energy difference on the two sides of the junction to the photon energy. We assume the detector is DC current biased at I_1, which we take to be the point with the maximum dynamic resistance $R_D = dV/dI$. R_D and I_1 are found from the DC transport curves (e.g. Fig. 1 left) of [4] and are plotted as function of temperature in Fig. 1 (right). The shift results in a DC output voltage $\delta V_{out} = R_D \delta I_1$, and this response is proportional to absorbed power. With impedance mismatch between antenna and load already accounted for in COMSOL, the absorbed power is $I_{THz}^2 R$ = 13.5 μW at 1.25 THz. Assuming the VI curve for T ~ 0.3 K, a temperature for which He^3 optical cryostats are commercially available (e.g. QMC and IR Labs), we obtain from Fig. 1 (center), and the given equations, a responsivity = 7 MV/W. Responsivity determined from the COMSOL simulation is plotted vs temperature as solid black symbols in Fig. 1 (right). Responsivity is ~10x smaller at T = 1.7 K than at 0.3 K.

Alternatively, the *coupled* power responsivity for a JJ detector is $S = R_D/2I_1R\Omega^2$, where $\pi\Omega$ approximately equals the ratio of photon energy to gap [3]. At 1.25 THz, Ω ~ 5. The impedance of the bowtie acting as a current source is 300 Ω at the 1.25 THz resonance, so that it will deliver 55% of the absorbed optical power to an 800 Ω load at its feed. Accounting for this mismatch, we obtain the responsivity curve given by open square symbols in Fig. 1 (right). The results agree well with those of the COMSOL simulation over most of the temperature range. Since the impedance of a bowtie can be adjusted by changing its shape, responsivity can be improved.

By expanding the V-I data from [4], we find the broad-spectrum noise amplitude to be ~1 μV. Thus, the noise equivalent power is not worse than 0.1 pW, and it would be much better if we restricted the noise spectral bandwidth to just 1 Hz, as is usually done via lock-in detection. An NEP of 0.1 pW, corresponds to a photon flux at 1.25 THz of ~1 photon every 5 ns. The prospects for single photon detection seem good.

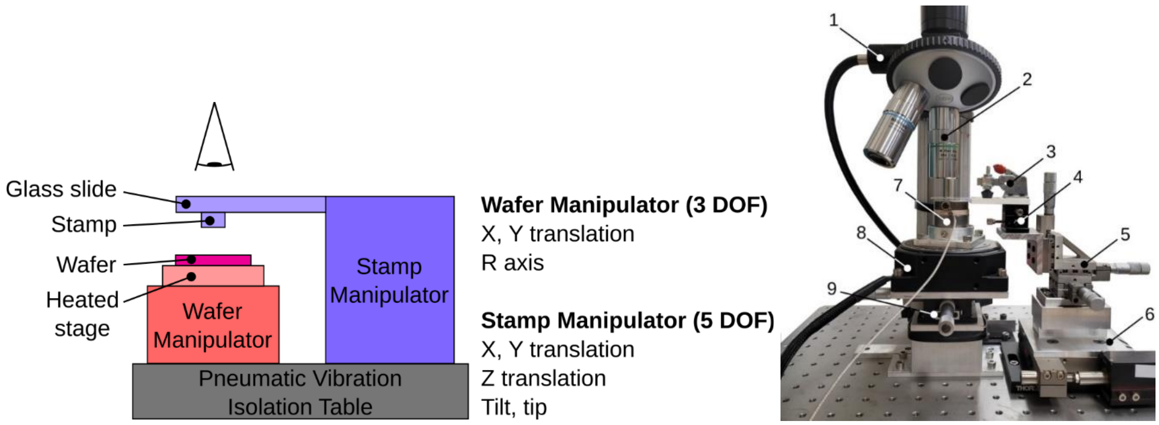

Fig. 2. (left) Schematic of stacking station. (right) Photograph of the stacking station. The primary components are the optical microscope with (1) a fiber-guided, in-line white illumination source and (2) long focal-length, plan apochromat, infinity-corrected objectives; the stamp manipulator with (3) a toggle clamp, (4) a tilt-tip goniometer, (5) 3-axis translation stage, and (6) a long-throw, motorized translation stage; and the wafer manipulator with (7) a heated vacuum chuck, (8) a motorized rotation stage, and (9) a 2-axis translation stage

Fabrication

Magic angle graphene may be produced by polymer-assisted and van der Waals material-assisted stamp transfer. We first fabricated inverted pyramidal trunk stamps from polydimethylsiloxane (PDMS) using the method described in [6] by casting PDMS into pyramidal molds etched in silicon and patterned by contact photolithography. After unmolding, the pyramidal PDMS is placed at the end of a glass slide handle and is then covered with a thin sheet of poly(bisphenol A carbonate) (PC).

Next, monolayer graphene flakes are stacked with "magic" angular alignment. To ensure accuracy in the rotational alignment, one may first slice a graphene flake into two pieces [7], guaranteeing that both flake pieces have the same initial orientation. We are able to exfoliate monolayer graphene flakes up to 50 μm in size, with monolayer thickness verified by micro Raman spectroscopy. We also demonstrated that they could be sliced in half using a tungsten scribe attached to a micromanipulator. Fig. 2 (left) presents a schematic of our graphene stacking station. The Wafer Manipulator has 3 degrees of freedom, namely x,y translation and rotation about a vertical axis with 4 mrad accuracy. The Stamp Manipulator has 5 degrees of freedom, namely x,y,z, tilt, and tip. Fig. 2 (right) presents a photograph of the completed stacking station.

We used our stacking station to demonstrate pick-up and aligned transfer of a multilayer graphene flake on top of another, shown in Fig. 3. Fig. 3(a) presents an optical micrograph of a multilayer graphene flake exfoliated on SiO_2 (280nm)/Si wafer. The PDMS stamp is aligned over the flake (Fig. 3b), and then engaged with the flake at room temperature (Fig. 3c). The sample is heated to 90°C, which increases the stickiness of the PC film, and the stamp is subsequently disengaged from the wafer. The flake attaches to the PC film and is lifted away from the SiO_2 substrate (Fig. 3d). Once a second multilayer graphene flake is identified (Fig. 3e), the first flake is aligned and engaged with the second flake (Fig. 3f). To release the first flake onto the second, the sample is heated to a temperature of 175°C, which melts the PC film and detaches it from the PDMS (Fig. 3g). Finally, the sample is cooled, removed from the transfer station, and is gently soaked in chloroform for 10 minutes to remove the PC. The resulting stack shown in Fig. 3h. In our system, we find that we can comfortably align two flakes within about 2 μm of a target alignment.

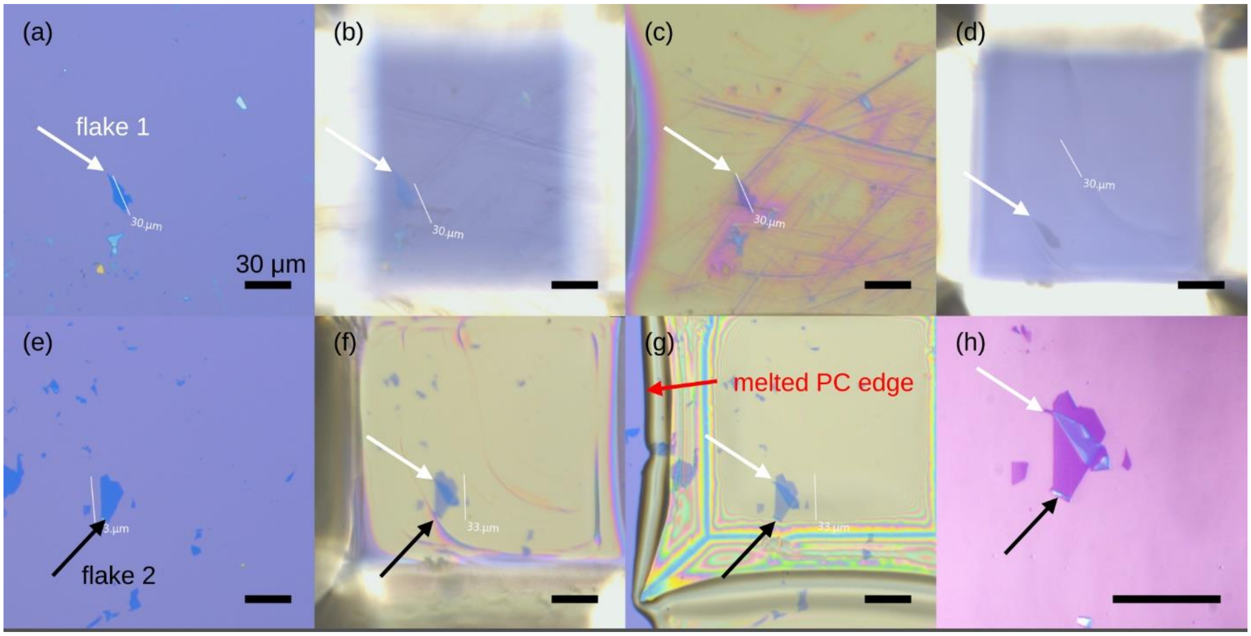

Fig. 3 Stacking of multilayer graphene using our stacking station.

After fabrication of magic angle graphene, contacts for bias control of the Fermi level and creation of the JJ weak link will be fabricated by electron-beam lithography. Bowtie antennas will be fabricated by contact photolithography. We will first measure the electronic properties of the magic angle graphene in a 0.3 K cryostat. First optical measurements will be performed using a Janis 8DT cryostat with immersion in pumped superfluid He at 1.7 K. The source will be a backward wave oscillator (Microtech Instruments) tunable from 160 GHz to 1.4 THz.

Summary

Estimate of responsivity for a bowtie-antenna-coupled graphene Josephson junction video detector was made. The estimated noise equivalent photon flux is promising for the ability to detect single photons. The non-thermal detection mechanism is expected to be sufficiently fast that the signal from signal photons should not be "smeared out." Such detectors may have future value for quantum information applications in the 5G and 6G bands.

Acknowledgements, disclosure, and data availability

This work was supported by Army OSD STTR contract # W911NF22P0026.

Conflict of interest statement

R. E. Peale and C. J. Fredricksen have ownership in Truventic and may benefit financially from the results of this research. Otherwise, all authors certify that they have no affiliations with or involvement in any organization or entity with any financial interest or non-financial interest in the subject matter or materials discussed in this manuscript.

Data availability statement

Truventic holds data rights under its STTR contract, but data is available from the authors upon reasonable request.

References

1. M. D. Eisaman, J. Fan, A. Migdall, and S. V. Polyakov, "Invited Review Article: Single-photon sources and detectors," Rev. Sci. Instr. 82, 071101 (2011), https://doi.org/10.1063/1.3610677
2. V. F. Guedes, F. A. Mendonca, J. B. R. Silva, R. V. Ramos, "Discrete variable quantum key distribution in millimeter-wave and THz regions," TechRxiv. Preprint. (2021), https://doi.org/10.36227/techrxiv.15091338.v1
3. P.L. Richards, "The Josephson Junction as a Detector of Microwave and Far-Infrared Radiation," Chapter 6 in Semiconductors and Semimetals Volume 12, edited by R.K. Willardson and Albert C. Beer (Elsevier, 1977), Pages 395-440.

4. J. M. Park, Y. Cao, L. Q. Xia, L-Q, Xia, S. Sun, K. Watanabe, T. Taniguchi, and P. Jarillo-Herrero, "Robust superconductivity in magic-angle multilayer graphene family," Nat. Mater. 21, 877 (2022), https://doi.org/10.1038/s41563-022-01287-1
5. A. Barone and G. Paterno, Physics and Applications of the Josephson Effect (Wiley-Interscience, 1982), Ch, 11.
6. A. C. Gadelha, D. A. A. Ohlberg, F. C. Santana, G. S. N. Eliel, J. S. Lemos, V. Ornelas, D. Miranda, R. B. Nadas, K. Watanabe, T. Taniguchi, C. Rabelo, P. Paulo de Mello Venezuela, G. Medeiros-Ribeiro, A. Jorio, L. G. Cançado, and L. C. Campos, "Twisted Bilayer Graphene: A Versatile Fabrication Method and the Detection of Variable Nanometric Strain Caused by Twist-Angle Disorder," ACS Appl. Nano Mater. 4, 1858 (2021), https://doi.org/10.1021/acsanm.0c03230
7. L D Varma Sangani, R S Surya Kanthi, P. C. Adak, S. Sinha, A. H Marchawala, T. Taniguchi, Kenji Watanabe and M. M, Deshmukh, "Facile deterministic cutting of 2D materials for twistronics using a tapered fibre scalpel," Nanotechnology 31, 32LT02 (2020), https://doi.org/10.1088/1361-6528/ab8b93
8. F. Xia, M. Gevers, A. Fognini, A. T. Mok, B. Li, N. Akabri, I. Esmaeil Zadeh, J. Qin-Dregely, C. Xu, "Deep confocal fluorescence microscopy with single-photon superconducting nanowire detector," Proc. SPIE 12089 (2022), https://doi.org/10.1117/12.2620775
9. V. B. Verma, B. Korzh, E. Wollman, Y. Zhai, A. Walter, E. Schmidt, A. Lita, J. Allmaras, M. D. Shaw, R. P. Mirin, S. W. Nam, "Superconducting nanowire single photon detectors and detector arrays in the mid-infrared," Proc. SPIE 12089 (2022), https://doi.org/10.1117/12.2619230